Nonlinear Analysis of Pretwisted Rods Using "Principal Curvature Transformation," Part II: Numerical Results

Aviv Rosen,* Robert G. Loewy,† and Mathew B. Mathew‡
Rensselaer Polytechnic Institute, Troy, New York

This, the second part of a two-part paper, makes use of the method developed in the first part to investigate the nonlinear behavior of rods. A first example illustrates the complexity of the nonlinear relative to the linear case. A second example examines such aspects as convergence of the iterative solution, the number of generalized coordinates needed, and four different levels of nonlinearity. A comparison of the results calculated using the theory for the second example with existing experimental results shows good agreement. A third example deals with the resulting moment distribution along the rod. Three methods for calculating the components of this resultant moment are presented, compared, and discussed. The fourth example involves the nonlinear behavior of a pretwisted rod.

I. Introduction

IN the first part of this paper, a numerical model for analyzing the nonlinear coupled bending-torsion of pretwisted rods was derived.[1] This model results from combining a "principal curvature transformation" and a generalized coordinates technique. Several advantages of the new model were cited in Ref. 1, but the best test of any new method is to make calculations the results of which can be checked against available experimental data or against those of earlier theories.

After a general description of the numerical solution procedure, four specific examples are dealt with here. The first is a special case that provides a vehicle for discussing the complexities associated with the nonlinear behavior of rods. The second case is a flat rod, loaded by a concentrated transverse force at its tip, whose characteristics were chosen to be the same as those for which experimental and theoretical results of other investigators are available in the literature. The deflections and rotations calculated using the present method are compared with the earlier results. The third case is another rod with zero pretwist for which the bending moment distributions along its length are calculated by three methods: the first two methods involve curvature and twist, which are calculated in two different ways. The third method integrates moments in terms of external loads along the rod, including all nonlinear effects. The results of the three moment distribution prediction methods are compared and discussed. The fourth example presents the behavior of a pretwisted cantilevered rod with a transverse load at its tip. All four are examined with the intent of assessing the accuracy and efficiency of the new method.

II. Generalities Concerning the Numerical Calculations

The Galerkin integrals, which result from the current formulation,[1] can be calculated by a variety of numerical integration schemes. In this paper, they are calculated using the IMSL DCADRE subroutine. This subroutine uses "cautious adaptive Romberg" extrapolation.[2]

All examples in this paper are for a cantilevered rod with constant distributed properties; i.e., bending stiffness in the η and ξ directions $(EI_{\eta\eta})$, $(EI_{\xi\xi})$, respectively; torsional rigidity (GJ); mass per unit length (m); and polar moment of inertia per unit length (MI_p). (For further definitions of symbols see Ref. 1.) The first three rods have zero pretwist; the fourth example includes pretwist. The shape functions $FV_{e(j)}$, $FW_{e(k)}$, $FV_{(j)}$, and $FW_{(k)}$ are chosen as the appropriate (jth or kth) mode shapes of free transverse vibration of a uniform, nonrotating clamped/free rod in a vacuum. Analytic expressions for these modes and the appropriate frequencies can be found, for example, in Ref. 3. The shape functions $F\phi_{e(\ell)}$ or $F\phi_{(\ell)}$ are chosen as the ℓth mode shape, of the free, in vaccuo torsional vibrations of a uniform fixed/free rod (see, for example, the analytic expressions in Ref. 4). Similarly, the shape functions $FU_{(n)}$ are chosen as the mode shapes of axial vibration of a fixed/free uniform rod.[3]

The generalized stiffness matrix is assembled using Eq. (23) of Ref. 1. Matrices and submatrices that are not functions of the unknown response are calculated only once and kept on a disk, thus increasing the efficiency of the solution procedure.

The system of equilibrium equations [Eq. (48) of Ref. 1] is nonlinear. In all cases presented here, this system is solved by a simple iterative procedure. At low loads, the last solution is used as an input to the next iteration. At higher loads, a relaxation factor is usually required to speed convergence. In these cases, the input to the new iteration is chosen at some point between the input and output of the last iteration. The exact value of the relaxation factor is not a critical parameter, and it influences only the number of iterations required for convergence, not the results themselves.

In all of the results presented here, the convergence condition was that the relative change of the displacement components or rotation at the tip $(v_{tip}, w_{tip}, \phi_{tip})$ between two subsequent iterations be less than 1%. Tighter requirements for convergence were also tried (e.g., relative change of >0.001 and less). The final results showed practically no change, but the computational time was increased significantly.

In order to save computational effort, the term $[K_2]\{q\}$ on the left-hand side of Eq. (48) in Ref. 1 was transferred to

Received Sept. 19, 1985; revision received June 25, 1986.

*Senior Postdoctoral Fellow. On sabbatical leave from the Department of Aeronautical Engineering, Technion—Israel Institute of Technology, Haifa, Israel. Member AIAA.
†Institute Professor. Fellow AIAA.
‡Graduate Student.

the right-hand side of the equation and added to the "loading vector" $\{f_s\}$. The coefficient matrix on the left-hand side of the equation is then no longer a function of the unknowns and it need be inverted only once at the beginning of the solution and can then be used throughout the solution procedure.

Four different mathematical models are used here. They are defined as follows (equations cited are in Ref. 1):

1) Model A—The curvature components and twist expressions contain only the terms of Eqs. (24) that are not underlined.

2) Model B—All of the terms of Eqs. (24) are included except for the last, fourth-order term in Eq. (24c).

3) Model C—All of the terms of Eqs. (24) are included.

4) Model D—Equations (A13-A15) are used for K_y, K_z, and T, respectively.

To limit what would otherwise be a very large number of results, a "standard mathematical model" was defined. It consists of model D and the combination of generalized coordinates: $N_v = N_w = N_{ve} = N_{we} = 3$, $N_\phi = N_{\phi e} = 5$. Unless otherwise stated, the theoretical results that are presented in what follows are for this "standard mathematical model."

III. Complexity of Nonlinear Relative to Linear Cases

This section attempts to provide insight as to the complexity of nonlinear compared with linear cases and to suggest the extra caution and accuracy required in analyzing them relative to their better known linear behavior. The rod considered in this section is shown in Fig. 1; a cantilevered, flat (zero pretwist) rod loaded by a concentrated force P_c at its tip. P_c lies in a plane parallel to the y-z plane and forms an angle γ with the undeformed y direction. The orientation of the y and z axes coincides with the principal directions of the cross section. The rod properties are:

$$(EI_{\eta\eta}) = (EI_{\zeta\zeta}) = 2.26684 \text{ N-m}^2; \quad (GJ) = 0.48659 \text{ N-m}^2$$

$$m = 0.02829 \text{ kg/m}, \quad MI_p = 0.04754 \times 10^{-6} \text{ kg/m} \qquad (1)$$

and are uniform along its length L of 0.508 m (20 in.). This is denoted "rod I" in what follows.

Since $(EI_{\eta\eta}) = (EI_{\zeta\zeta})$, any arbitrary orthogonal directions of the cross section are principal directions. This rod will, therefore, always bend in the plane defined by the axes x and P_c. As a result of this symmetry, one would expect torsion not to occur even with large deflections.

Two rod I, "standard mathematical model" cases were calculated; for $\gamma = 0$ and 45 deg. In Fig. 2, v_{tip} and w_{tip} (components of tip displacement in the directions y and z, respectively) are plotted as functions of the tip load. As expected, when $\gamma = 0$, w_{tip} is equal to zero; for $\gamma = 45$ deg, v_{tip} and w_{tip} are equal; and their resultant $(v_{tip}^2 + w_{tip}^2)^{1/2}$ is practically equal to v_{tip} when $\gamma = 0$ deg at low loads, with small deviations (not exceeding 4%) occurring at higher loads where the inaccuracies of the model increase. In the usual linear theory of rod bending, this symmetric analytical behavior results because a symmetric system of equations is obtained for the case $\gamma = 45$ deg, where v and w can be interchanged without changing the equations. On the other hand, in the nonlinear case, as a result of introducing finite rotations, the mathematical model is not symmetric for $\gamma = 45$ deg. This lack of symmetry can be seen clearly in the expressions for the curvature components K_y and K_z [see Eqs. (A13) and (A14) of Appendix A of Ref. 1], where equal expressions for v and w will give only equal values of K_y and K_z if ϕ takes on appropriate values. Since v_{tip} and w_{tip} are shown as equal in Fig. 2, in accordance with physical reasoning, it appears that the method behaves properly. The fact that particular values of ϕ are required to provide symmetry in expressions for v and w shows that there is dissymmetry in the mathematical model itself.

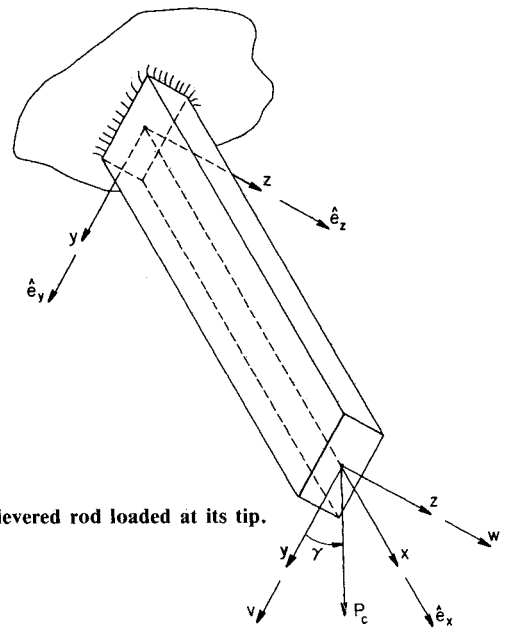

Fig. 1 Cantilevered rod loaded at its tip.

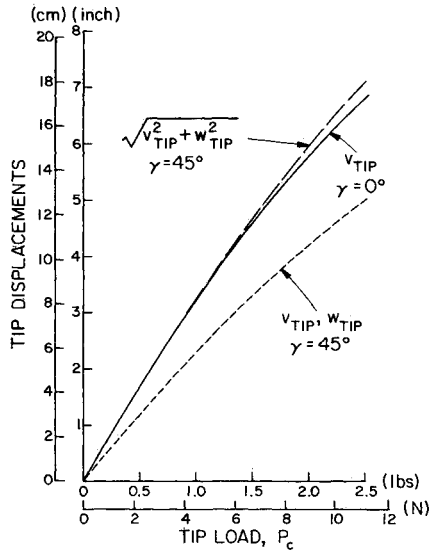

Fig. 2 Rod I—Tip displacement as a function of tip load.

In Fig. 3a, ϕ_{tip} is plotted vs load magnitude for $\gamma = 45$ deg. Clearly, for $\gamma = 0$ deg, ϕ_{tip} is identically zero. Does this mean that, in spite of physical reasoning, the cases of $\gamma = 0$ and 45 deg give different results? If so, one would suspect that the model is incorrect. The answer is that ϕ is one of three Euler angles that are part of the mathematical model. If the sequence of the assumed rotations assumed to achieve a state of deformation is changed, then the values of these rotations change, although the deformed state remains the same. Euler angles, for all their utility in solution procedures, do not represent basic invariant properties of deformed rods. This matter is also discussed in Ref. 5. A better representative of rod rotations due to deformation is the matrix $[T_{EIE}]$, which is defined by Eq. (A1) of Ref. 1. (For more details see Ref. 6.)

One concludes that in nonlinear response, contrary to the linear case, the existence of an angle ϕ does not necessarily indicate torsion along the rod. In Fig. 3b, an expression for the twist distribution along the rod at a load of $P_c = 11.12$ N and $\gamma = 45$ deg is plotted according to the right-hand side of Eq. (A16c) of Ref 1, i.e., calculated from the series expression for v, w, and ϕ. Note that the equivalent of Eq. (A16c)

of Ref. 1 does not apply at all points along the rod in a Galerkin method, but is satisfied only on the average. The result of using the left-hand side of Eq. (A16c)—i.e., calculated from the series expression for ϕ_e—gave even smaller values, which practically coincide with the zero axis and are, therefore, not shown in Fig. 3b. It is shown, therefore, that these values of twist also approach zero, as in the case where $\gamma=0$ deg. Further discussion of these two methods of calculating T appears in Sec. V. Figure 3b also shows the distribution of $\phi_{,x}$, which represents twist in the linear case. It can be seen that unlike T, $\phi_{,x}$ is nonzero, even on the average, thus indicating that ϕ is not related directly to torsion as it is in the linear case. To show that, in this case, ϕ is an artifice (resulting from the choice of coordinates and nonlinear contributions due to rod bending) in another way, the torsional stiffness of the rod (GJ) was increased by a factor of 10 holding all other properties constant and displacement and rotation results recalculated. These values of v, w, and ϕ were too close to those presented in Figs. 2 and 3a for differences to be seen in the graphs. Clearly, for this nonlinear case, ϕ is not solely associated with torsion, in contrast to what is expected from linear behavior.

IV. Comparison of Results with Experiment for Different Nonlinear Models

To further validate the mathematical model, differences among them (models A-D) were investigated and their results compared with those in the literature, including test data. The case under consideration is, again, a cantilevered rod loaded by a tip force (see Fig. 1). In addition, a uniformly distributed load along the rod, corresponding to its own weight, is accounted for. Although the influence of the self-weight is very small for the case in question and can be neglected at high loads, it is included here for completeness. Thus, mathematically, the distributed load is described as follows (see Fig. 1):

$$\bar{P}=[mg+P_c\delta(x-L)](\cos\gamma\hat{e}_y+\sin\gamma\hat{e}_z) \qquad (2)$$

where g is the gravity acceleration.

These calculations include "rod II," a flat aluminum rod which is one of the models (beam 2) of Ref. 8 and is identical to those considered and presented in Refs. 9 and 10. Its properties are listed in Table 1. The stiffness properties of the rod were based on the test results of Ref. 9 noting that, when $\gamma=0$, the v displacement is small and behaves linearly under loads in the range of interest. The experimental slope of the curve of v vs P_c ($\gamma=0$ deg) was used to calculate ($EI_{\eta\eta}$), and ($EI_{\zeta\zeta}$) was obtained by multiplying ($EI_{\eta\eta}$) by the ratio of thickness to width squared. The torsional rigidity (GJ) was calculated first by using the expression [$G=E/2(1+\nu)$], where Poisson's ratio is 0.31, and using the area properties of a rectangular cross section to estimate J. Then (GJ) was recalculated, based on the first natural torsional frequency of the rod, as given in Ref. 10. There was a difference of a few percent between the two values, and (GJ) was taken as the average.

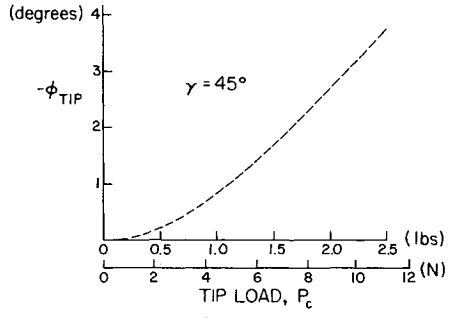

Fig. 3a Rod I—Euler angle ϕ as a function of tip load.

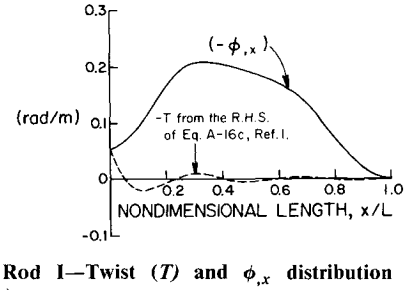

Fig. 3b Rod I—Twist (T) and $\phi_{,x}$ distribution ($P_c=11.12$ N, $\gamma=45$ deg).

Calculations using different numbers of generalized coordinates were run to check the convergence of the truncated series, which describes the displacement and principal curvature components. Good convergence was obtained whenever more than one mode was used in each type of deformation; in-plane bending, out-of-plane bending, and torsion. In the authors' experience, the convergence of the present method is better than that usually obtained using a direct Galerkin solution of equilibrium equations.[7] Some of the results and more details are presented in Ref. 6.

Figure 4 compares the results obtained using the four mathematical models (A-D) described in Sec. II. In these figures, v_{tip}, w_{tip}, and the "tip twist angle" $\tilde{\phi}_{tip}$ (see Appendix) are presented, as predicted by the four different models. A comparison with the experimental results of Refs. 8 and 9 is also shown. The following conclusions can be drawn from these figures:

1) The fourth-order term that constitutes the difference between mathematical models B and C has a negligible effect in all of the cases calculated.

2) Nonlinear terms cause an increase in the edgewise component of the displacement (see Fig. 4a) relative to the linear theory case. Mathematical models A-C give results that are close to one another and higher than the results of model D. There is good agreement between the experimental results for edgewise displacement and the predictions using model D.

3) Mathematical models A-C give practically identical results for the flatwise component of displacement, which are higher than the linear predictions (Fig. 4b). Mathematical model D predicts smaller flatwise displacements than the linear theory, and they are close to the experimental values.

4) Mathematical models A and B predict different "twist angles" $\tilde{\phi}$ at high loads, with the latter yielding smaller values. (See Fig. 4c.) Model D results are even lower and agree quite well with the experimental measurements (better than the other models) at all but the highest loads. These predictions for $\tilde{\phi}$ are based on the arc tan formulation [Eq. (A4)].

5) None of the present theoretical models results in a divergence of the type suggested by figures shown in and applying the results of the theory of Refs. 8-10 and discussed later in this paper in connection with Fig. 5. To the contrary, convergence has been obtained easily, even at the highest postulated loads.

Table 1 Properties of rod II

Length L, m (in.)	0.508 (20)
Width, m (in.)	0.0127 (0.5)
Thickness, m (in.)	0.003175 (0.125)
Principal bending stiffness components	
($EI_{\eta\eta}$), N-m^2	36.2695
($EI_{\zeta\zeta}$), N-m^2	2.2668
Torsional rigidity (GJ), N-m^2	2.9623
Mass per unit length m, kg/m	0.11317
Mass moment of inertia per unit length (MI_p), kg-m	1.6162×10^{-6}

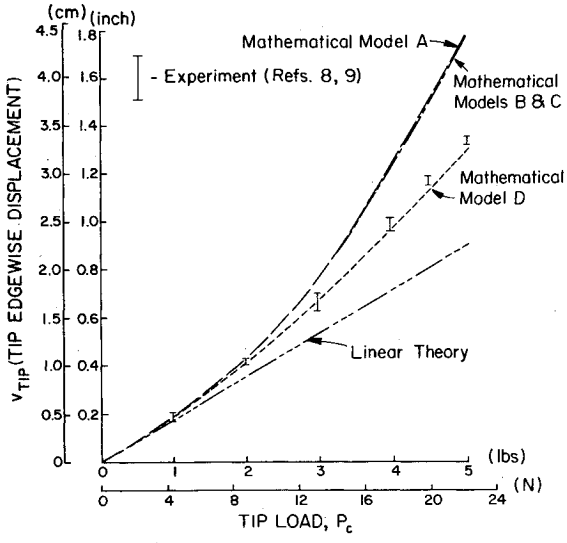

Fig. 4a Rod II—Result comparison for edgewise displacement ($\gamma = 30$ deg).

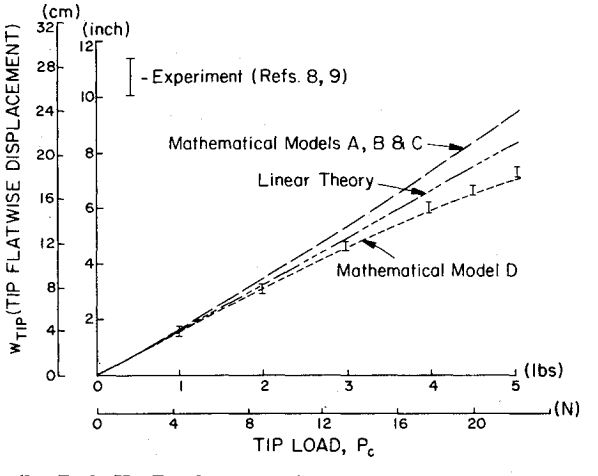

Fig. 4b Rod II—Result comparison for flatwise displacement ($\gamma = 30$ deg).

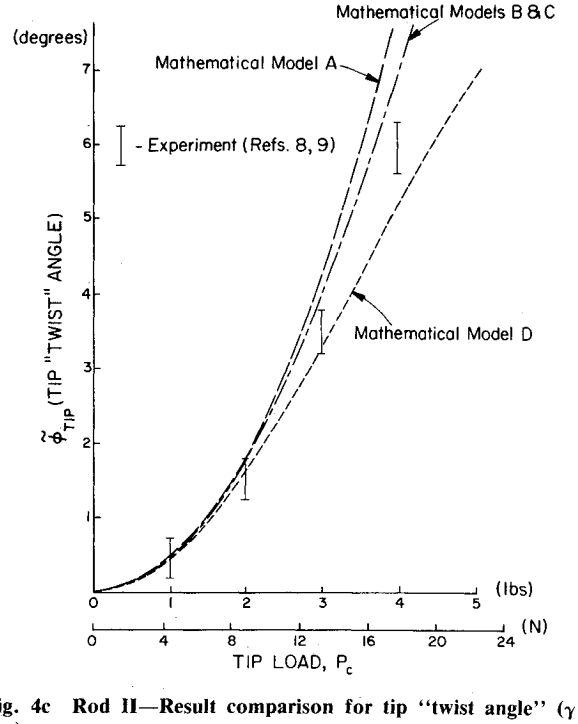

Fig. 4c Rod II—Result comparison for tip "twist angle" ($\gamma = 30$ deg).

Calculations performed for other values of the load application angle γ showed trends similar to those discussed previously, but are omitted for brevity's sake.

Figure 5 compares the results of several theoretical predictions for and experimental measurements of tip deflection as a function of the load angle γ for several load levels. The present theoretical results for the edgewise and flatwise components exhibit good agreement with the experimental results for all of the tip loads and load angles tested. Similar graphs for the twist angle $\tilde{\phi}$ are presented in Fig. 5c. The nature of $\tilde{\phi}$ is discussed in the Appendix [values of $\tilde{\phi}$ were calculated using the arc tan and arc cos formulations, Eqs. (A4) and (A5), respectively]. Only small differences result and they are apparent in the region 0 deg $< \gamma <$ 45 deg only at the highest loads. Agreement between theoretical and experimental results is good for the two lower loads, while some discrepancies appear at the highest load for γ angles near 45 deg. In general, the agreement between the results of the present theory and experiment is better than those presented for the theoretical results in Refs. 9 and 10. Moreover, as noted earlier, in all of the cases examined here, good convergence is obtained using a simple iterative procedure, whereas the theory of Refs. 9 and 10 appears to predict diverging tip deflections at certain loads (not shown in the experiments). It is noteworthy that a more complicated Newton-Raphson method is also required in Refs. 9 and 10 to solve the nonlinear problem.

To check self-consistency within the present model, the values of $(EI_{\eta\eta})$ and $(EI_{\zeta\zeta})$ were interchanged and nonlinear rod deformations recalculated. It is clear from physical reasoning that this should give the same results as the previous calculations, if the load angle is replaced by (90 deg $-\gamma$). As noted earlier, such would not be a trivial result of identical calculations, as it would be in the linear case, since the present nonlinear model is not symmetric with respect to y and z. Failure to obtain this expected behavior would be an indication of inaccuracies in the derivation. Practically identical results, however, are obtained for the tip edgewise and flatwise displacements. In the case of the tip "twist angle" $\tilde{\phi}$, identical results are obtained at the two low loads, while small deviations appear at the high load. [See the result of Eq. (A6) in Fig. 5c.] These deviations probably result from the very large deformations in that region and would probably disappear if a still more accurate nonlinear analysis were used.

To this point only tip deflections and rotations have been presented in this paper. The spanwise distributions of these variables were also calculated and good agreement with the experimental resuts given in Ref. 9 obtained for those distributions. These results are not presented here to conserve space.

V. Resultant Moment Distributions

In many engineering applications, the calculation of the cross-sectional moment or maximum stress is of prime importance. The purpose of this section is to present theoretical results for the moment distributions along the rod. Such moments are calculated by three methods—described in more detail in Appendix B of Ref. 6—and which include:

1) Method A—Integrating the appropriate product of loads along the rod times their lever arms.

2) Method B—Calculating the curvature and twist by using the v_e'', w_e'', and ϕ_c' series [the direct principal curvature expressions, see Eqs. (14) of Ref. 1].

3) Method C—Using displacement derivatives to express the curvature and twist according to Eqs. (A13-A15) of Ref. 1.

The moment distribution calculations were performed for a cantilevered rod called "rod III" in what follows. Its properties are: $L = 0.35$ m, $(EI_{\eta\eta}) = 478.5$ N-m^2, $(EI_{\zeta\zeta}) = 0.538$ N-m^2, $(GJ) = 0.8032$ N-m^2, and $\gamma = 15$ deg.

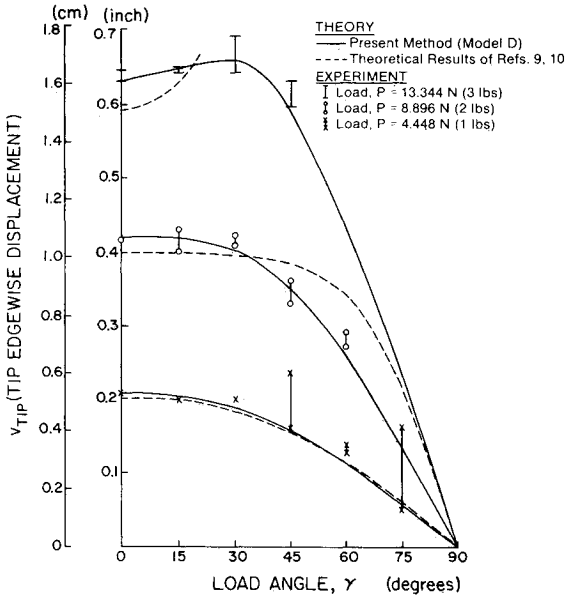

Fig. 5a Rod II—Comparisons among calculated and experimental results for edgewise components of tip displacement.

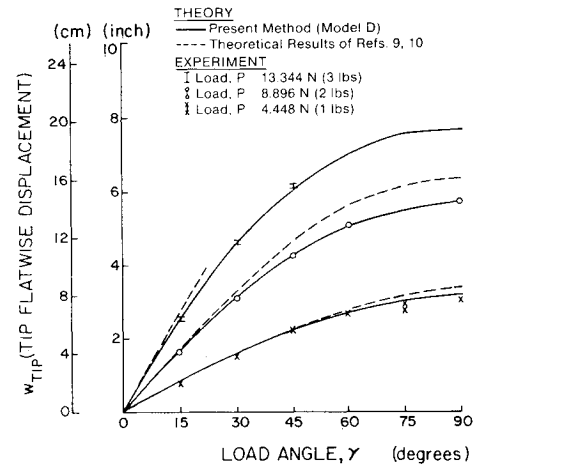

Fig. 5b Rod II—Comparisons among calculated and experimental results for flatwise components of tip displacement.

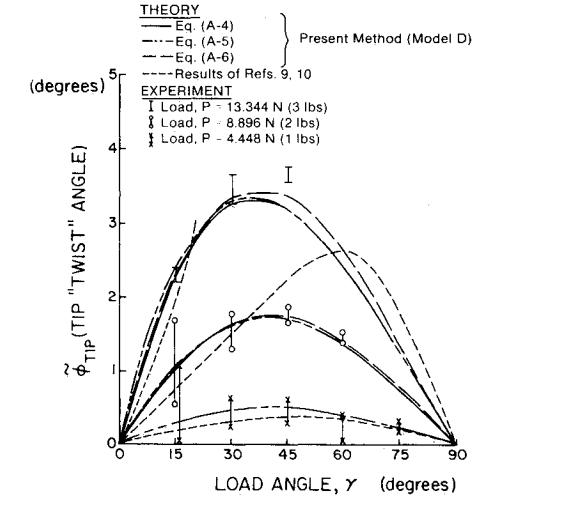

Fig. 5c Rod II—Comparisons among calculated and experimental results for tip "twist angle."

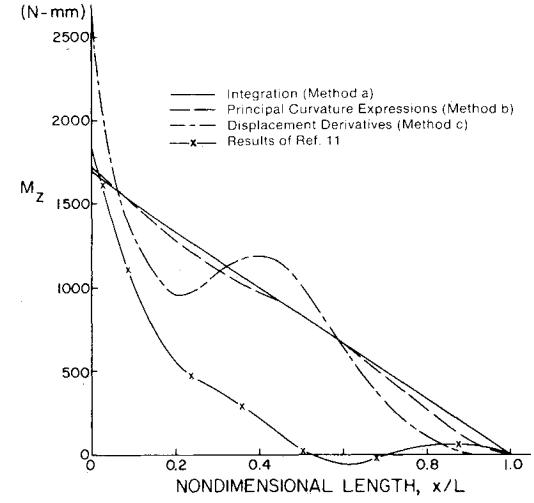

Fig. 6 Rod III—Edgewise bending moment distributions.

Here the influence of self-weight is neglected. These properties have been chosen to allow comparison of the results of present calculations with those presented in Ref. 11.

The spanwise distributions of moment components for a load of $P_c = 5$ N were calculated. In the case of the components M_x and M_y (in the directions $\hat{e}_{x1}$ and $\hat{e}_{y1}$, torsional and flatwise components, respectively), the results of methods B and C coincide and show good agreement with method A. (For details, see Sec. 5 of Ref. 6.)

The spanwise distribution of the edgewise component M_z (in the $\hat{e}_{z1}$ direction) is shown in Fig. 6. Agreement between methods A and B is good, but the results of method C oscillate about the monotonic results of the other two methods, with deviations at the root exceeding 50%. Some insight can be gained by examining the theoretical results of Ref. 11 for the same case. Reference 11 (similar to Ref. 7) solves the equilibrium equations by direct application of a Galerkin method, and the resulting moment components are calculated using expressions similar to those of method C. Distributions of M_x and M_y in Ref. 11 are similar to the present results. The Ref. 11, M_z distribution shown in Fig. 6 used $N_v = N_w = 4$, $N_\phi = 5$ in the series solution, and large discrepancies appear compared with the other results. The difficulties in predicting M_z by method C and that in Ref. 11 arise because the expression $w_{,xx}\phi$ in the equation for K_y [see Eq. (A13) of Ref. 1] becomes of the same order of magnitude as the linear term due to large differences in the magnitudes of v nd w. The better results obtained using principal curvature expressions (method B) are also in agreement with the results of Sec. III, concerning the twist distribution.

VI. Behavior of a Pretwisted Rod

The pretwisted rod considered here is identical to rod II of Sec. IV, except that it has a linear pretwist of 90 deg between its root and tip cross sections. The y axis coincides with the width direction of the root cross section. The rod is clamped at the root and free at the tip. A concentrated transverse load acts at the tip in *its* width direction.

Components of tip transverse displacements are shown in Fig. 7a as functions of the tip load. Here v is the component in the width direction of the root cross section, while w is perpendicular to it. Results obtained using nonlinear mathematical models A and D are presented together with those of an exact analytical solution of the linear equations of bending of a linearly pretwisted rod loaded by a transverse tip force. (The detailed analytic expressions appear in Ref. 12.) At small loads and small displacements the results of the exact linear theory coincide with the results of the present method. This proves that the pretwist is properly taken into

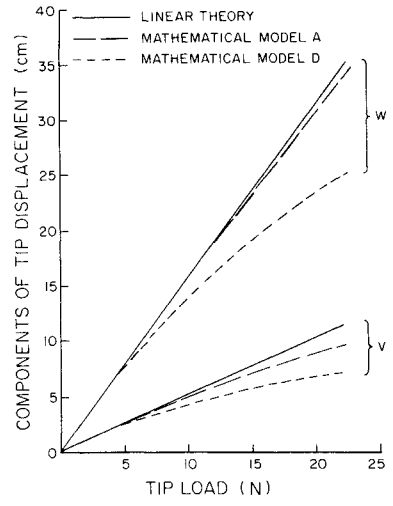

Fig. 7a Pretwisted rod—Components of the transverse displacement at the tip as a function of the tip load.

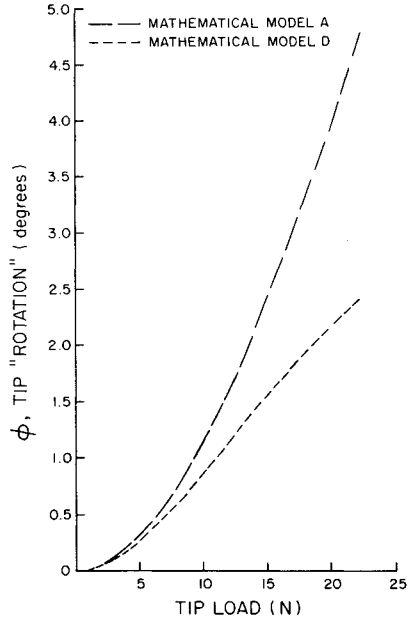

Fig. 7b Pretwisted rod—Angle ϕ at the tip as a function of the tip load.

account. As displacements increase, nonlinear effects begin to appear. In the present case, both deflection components decrease due to nonlinear effects. The decrease is larger for mathematical model D than for mathematical model A.

It is noted that the trend of nonlinear effects depends on structural properties, amount of pretwist, and tip load direction. Changes of tip load direction or amount of pretwist were shown to increase certain displacement components.

The angle ϕ at the tip is presented in Fig. 7b as a function of tip load. This angle, as noted earlier, results solely from nonlinear effects. Mathematical model D yields lower values than model A for the pretwisted rod, as was true for zero pretwist.

The amount of pretwist was chosen here to be larger than found in most practical cases, to check the accuracy of the present method. Results for the stability of axially compressed rods are presented for even larger values in Ref. 12. The latter calculations show that there is no problem in accounting for large amounts of pretwist (the tip cross section is rotated more than two revolutions relative to the root cross section) if the number of terms in the series for v, w, v_e'', and w_e'' is increased as pretwist becomes large.

VII. Conclusions

The following conclusions emerge from the studies reported here.

1) The nonlinear coupled bending-torsion case is much more complicated, its behavior is less evident, and it is deserving of special care, as compared with the linear case. The interpretation of results obtained in such cases is not straightforward.

2) Euler angles are useful mathematical tools for the purposes of derivation, but they cannot be measured directly during experiments.

3) In the nonlinear case, the presence of ϕ does not necessarily indicate the action of a twisting moment.

4) The results of mathematical model D show very good agreement with existing experimental results and, for the other cases examined, produced no apparent violations of simple physical reasoning.

5) The magnitude of discrepancies between the results produced using mathematical model D as compared with those obtained with mathematical models A–C increases with higher load levels. This indicates that neglecting products of elastic rotations is not justified in the ranges considered.

6) For all combinations of loads and loading angles investigated, very good convergence properties were obtained for the nonlinear system using a simple iterative procedure incorporating relaxation factors at high load levels. It has also been shown that two terms in each of various series which represent the unknowns, is enough to give a converged displacement solution of reasonable accuracy.

7) The resulting moment components calculated by integrating loads along the rod agree well with those obtained using principal curvature components.

8) The present method seems to be more efficient and more accurate than those in which the equilibrium equations are solved directly. Its success probably stems from a fortuitous combination of the "principal curvature transformation," the generalized coordinates technique, and a Galerkin method in which the curvature and twist components are used as weighting functions.

9) Results for pretwisted rods show good agreement with exact analytical results for the linear case, as long as the deformations are small. As the deformations are increased, nonlinear effects become important. The magnitude and even trends of such nonlinear effects may change with pretwist and load direction.

Appendix: "Twist Angles" as Measured in Experiments with Rod II

The authors of Refs. 9 and 10 present the results of measurements including what is referred to as the "twist angle." In order to compare their experimental results with those of the present theory, special examination of these angles is required. The purpose of this Appendix is, therefore, to consider their meaning.

In the research of Refs. 9 and 10, lightweight "reference rods" were attached in the chordwise direction normal to the rod centerline at each of four selected spanwise stations ($x=0.25L$, $0.50L$, $0.75L$, L). The exact length of the reference rods was 6.000 in. $\pm$0.001 in., they were quite stiff (see details in Ref. 9) and each weighed about 1.6 g. The influence of their weight on rod displacements is, therefore, negligible.

If the length of the lightweight reference rod is denoted d, then the vector describing this rod is

$$\bar{d}=d\hat{e}_{y1} \tag{A1}$$

As explained in Ref. 1 (see also Fig. 1), $\hat{e}_x$, $\hat{e}_y$, and $\hat{e}_z$ form a triad of unit vectors in the directions of the coordinate lines x, y, and z, respectively; $\hat{e}_{x1}$, $\hat{e}_{y1}$, and $\hat{e}_{z1}$ is the same triad after deformation. The transformation between both triads

is given by [see Eq. (A1) of Ref. 1]

$$\begin{Bmatrix} \hat{e}_{x1} \\ \hat{e}_{y1} \\ \hat{e}_{z1} \end{Bmatrix} = [T_{E1E}] \begin{Bmatrix} \hat{e}_x \\ \hat{e}_y \\ \hat{e}_z \end{Bmatrix} = \begin{bmatrix} S_{xx} & S_{xy} & S_{xz} \\ S_{yx} & S_{yy} & S_{yx} \\ S_{zx} & S_{zy} & S_{zz} \end{bmatrix} \begin{Bmatrix} \hat{e}_x \\ \hat{e}_y \\ \hat{e}_z \end{Bmatrix} \quad \text{(A2)}$$

The terms S_{ij} $(i,j=x,y,z)$ are functions of the displacements and their derivatives. These functions vary according to the levels of nonlinearity considered. The terms for the case of small strains and moderate elastic rotations are given in Refs. 7 and 13. The terms for a certain class of higher nonlinearity, where products of elastic rotations are not negligible compared to unity (model D), are given by Eq. (A9) of Ref. 1.

The blade "twist angle" $\tilde{\phi}$ is defined as that caused by tip loads, so that the experimental rod "twist angle" values are incremental angles measured against those that exist when no loads are applied ($P_c=0$).

Calculation of the angle $\tilde{\phi}$ refers to the projection of a particular rotated reference rod onto a plane parallel to the y-z plane (see Fig. 1). If the angle between this projection and the loading direction is denoted α, the $\tilde{\phi}$ is defined as

$$\tilde{\phi}=\alpha-\alpha_0 \quad \text{(A3)}$$

where α_0 is the initial value of α when $P_c=0$.

Using straightforward geometry (a detailed derivation appears in Appendix A of Ref. 6) expressions for α are obtained. In what follows, two different expressions are presented.

Based on an arc tan formulation, the expression for α becomes

$$\alpha=\arctan\frac{S_{yy}\sin\gamma-S_{yz}\cos\gamma}{S_{yy}\cos\gamma+S_{yz}\sin\gamma} \quad \text{(A4)}$$

If an arc cos formulation is used, then the expression is

$$\alpha=\arccos\frac{S_{yy}\cos\gamma+S_{yz}\sin\gamma}{\sqrt{S_{yx}^2+S_{yy}^2+S_{yz}^2}} \quad \text{(A5)}$$

In the exact case, Eqs. (A4) and (A5) will give identical values of α. But, because of inaccuracies due to approximations in the model and the numerical solution, certain discrepancies are expected. Because of such inaccuracies, the denominator of Eq. (A5) is not replaced by unity (its value in the exact case).

The derivation up to this point has been for the case shown in Fig. 1, where the larger cross-sectional moment of inertia is chosen to be about the Z axis. When the opposite occurs—when the system of coordinates is defined such that the moment of inertia is larger about the y axis—then the lightweight reference rod lies in the $\hat{e}_{z1}$ direction. The expression for α becomes, for the arc tan formulation,

$$\alpha=\arctan\frac{-S_{zy}\sin\gamma+S_{zz}\cos\gamma}{S_{zy}\cos\gamma+S_{zz}\sin\gamma} \quad \text{(A6)}$$

and using the arc cos formulation,

$$\alpha=\arccos\frac{S_{zy}\cos\gamma+S_{zz}\sin\gamma}{\sqrt{S_{zx}^2+S_{zy}^2+S_{zz}^2}} \quad \text{(A7)}$$

Acknowledgments

This research was supported by the Army Research Office through the Rotorcraft Technology Center at Rensselaer Polytechnic Institute under Contract DAAG 29-82-K-0093; Dr. Robert Singleton, Contract Monitor.

References

[1]Rosen, A., Loewy, R. G., and Mathew, M. B., "Nonlinear Analysis of Pretwisted Rods Using 'Principal Curvature Transformation'—Part I: Theoretical Derivation," *AIAA Journal*, Vol. 25, March 1987, pp. 470–478.

[2]deBoor, C., "CADRE: An Algorithm for Numerical Quadrature," *Mathematical Software*, edited by John R. Rice, Academic Press, New York, 1971, Chap. 7.

[3]Volterra, E. and Zachmanoglou, E. C., *Dynamics of Vibrations*, Charles E. Merrill Books, Columbus, OH, 1965.

[4]Bisplinghoff, R. L., Ashley, H., and Halfman, R. L., *Aeroelasticity*, Addison-Wesley, Reading, MA, 1957.

[5]Hodges, D. H., Ormiston, R. A., and Peters, D. A., "On the Nonlinear Deformation Geometry of Euler-Bernoulli Beams," NASA-TP 1566, April 1980.

[6]Rosen, A., Loewy, R. G., and Mathew, M. B., "A Method of Principal Curvature Transformation for Analyzing the Nonlinear Coupled Bending-Torsion of Pretwisted Rods—Part II: Numerical Results," Rensselaer Polytechnic Institute, Troy, NY, RTC Rept. D-85-3, 1985.

[7]Rosen, A. and Friedmann, P., "The Nonlinear Behavior of Elastic Slender Straight Beams Undergoing Small Strains and Moderate Rotations," *ASME Transactions, Journal of Applied Mechanics*, Vol. 46, 1979, pp. 161–168.

[8]Dowell, E. H. and Traybar, J., "An Experimental Study of the Nonlinear Stiffness of a Rotor Blade Undergoing Flap, Lag and Twist Deformations," Department of Aerospace and Mechanical Sciences, Princeton University, Princeton, NJ, AMS Rept. 1194, Jan. 1975.

[9]Dowell, E. H. and Traybar, J. J., "An Experimental Study of the Nonlinear Stiffness of a Rotor Blade Undergoing Flap, Lag and Twist Deformations," Addendum to Ref. 8, AMS Rept. 1257, Dec. 1975.

[10]Dowell, E. H., Traybar, J. J., and Hodges, D. H., "An Experimental-Theoretical Correlation Study of Non-Linear Bending and Torsion Deformations of a Cantilever Beam," *Journal of Sound and Vibration*, Vol. 50, No. 4, 1977, pp. 533–544.

[11]Rosen, A. and Neer, A., "Non-Linear, Non-Planar Deformations of Elastic Blades Under General Loading," Department of Aeronautical Engineering, Technion—Israel Institute of Technology, Haifa, Israel, TAE No. 421, Aug. 1981.

[12]Rosen, A., Loewy, R. G., and Mathew, M. B., "Elastic Stability of Pretwisted Rods," Rensselaer Polytechnic Institute, Troy, NY, RTC Rept. S-85-2, 1985.

[13]Rosen, A. and Rand, O., "Numerical Model of the Nonlinear Behavior of Curved Rods," *Computers and Structures*, Vol. 22, No. 5, 1986, pp. 785–799.